Structure of silica in matt water-based lacquer

C. P. Royall and A. M. Donald*
Cavendish Laboratory, University of Cambridge, Madingley Road, Cambridge CB3 0HE, United Kingdom
(Received 3 October 2001; published 22 August 2002)

A model for the structure of silica matting agent in water-based lacquers is presented. It is assumed that, during film formation, the air that lies between the silica particles in the dry powder is replaced by polymer. At a critical concentration this leads to a silica structure similar to that of the dry powder. We assume the bulk volume occupied by the dry silica powder (silica and air) equals the dried lacquer film (polymer, silica, and residual air). Since the silica structure in the dry powder percolates, the silica in the dried lacquer is tested for percolation. Experimentally, a percolation threshold is found close to the critical concentration predicted by the model. Two further silica structures are also seen under different conditions. At low silica concentrations, the silica particles are suspended in the lacquer matrix and isolated. Above the percolation threshold, where the bulk volume of the dry silica exceeds that of the film, the silica structure can undergo collapse. This is caused by volume reduction in the lacquer as water evaporates. The lacquer is imaged with confocal laser scanning microscopy, to produce three-dimensional images of the bulk of the 50-μm film. Resolution is enhanced with image reconstruction via deconvolution. Computational image analysis is then used to investigate the structure quantitatively.

DOI: 10.1103/PhysRevE.66.021406 PACS number(s): 83.80.Hj, 82.70.Dd, 81.30.−t

I. INTRODUCTION

Polymer lattices, the basis of many water-based lacquers, have been studied for half a century. Although the film-formation process from a latex suspension to a continuous polymer film is not fully understood, a number of mechanisms have been proposed. For film formation to proceed, the aqueous latex suspension is laid down on a substrate, and water is removed through evaporation, leaving a densely packed array of latex spheres. These deform to produce a continuous polymer layer. Typically this deformation occurs at the same time as water evaporates. On a longer time scale, polymer chains interdiffuse between the latex particles [1].

This work considers a somewhat different system. Although the matt lacquer used is based on a polymer latex, amorphous silica is included to produce a roughened surface. As the silica forms aggregate particles on the micron length scale, the surface roughness reduces specular reflection, or, in other words, it causes matting [2]. The relationship between matting and surface roughness will form the subject of a future publication. Here the underlying silica structure in the bulk of the film is considered.

To the authors' best knowledge, the only published work on this system is that of Schneider [2], who noted the reduction in reflection resulting from silica inclusions, but did not relate this to the microstructure of the film. Gate *et al.* [3] investigated the relationship between surface microstructure and this loss of reflection for generic lacquers. Previous work [4] shows that silica is present on the film surface. Here we seek to determine the structure of the silica in the bulk of the film.

A model will be developed to describe the structure taken up by the silica, which builds on earlier work [4]. During the formulation of the lacquer, silica is initially in the form of a dry powder but following film formation, it is incorporated into a polymer film. Essentially we assume that at a certain critical silica concentration, air between silica particles is effectively replaced by polymer, and consequently that the silica packing at this critical concentration is similar to that in the dry powder. A volume-based argument allows derivation of this silica concentration and determination of the critical mass fraction required.

The structure formed by the silica in the dried lacquer can be accessed with confocal laser scanning microscopy (CLSM) [5,6]. By eliminating out-of-focus contributions to the signal, CLSM can produce images within thick specimens. Combining a stack of two-dimensional (2D) images, a 3D image can be built up. The lacquer here is particularly appropriate for 3D imaging, as the silica and polymer are refractive index matched for end use reasons, with little absorption and scattering of the light, enabling high quality images to be obtained up to 100 μm into the specimen.

However, the resolution of CLSM is ultimately limited by diffraction. Since there is silica structure below this length scale, computational image reconstruction via deconvolution is used to enhance the resolution [5,7–9]. This reveals silica structure on a smaller scale than that directly accessible to the microscope. Image analysis techniques are then employed to extract quantitative data from the graphic images. The silica structure in these images may be modeled to a first approximation by randomly populating sites on a cubic lattice. Simulated images produced in this way are then analyzed in the same way as the experimental work.

II. LATEX FILM FORMATION WITH SILICA

Here we are interested in film formation in the presence of fumed silica. The 20-nm silica particles are weakly bound via hydrogen bonding into aggregate particles in the (1–10)-μm size range [10]. These aggregate particles are broken down under shear, but reform in a suspension at rest [11]. We therefore suppose that the silica particles may re-

*Author to whom correspondance should be addressed.

form in the lacquer following mixing, so that the silica is dispersed throughout the latex.

As water evaporation brings the smaller (80-nm) latex particles together, the larger silica particles are trapped in the latex matrix. The film-forming polymer latex used deforms at the same rate as the water evaporates [1]. Therefore, as the silica surface is dewetted by water evaporation, polymer takes its place, so capillary forces should not influence the individual silica particles too much during film formation. In any case, movement of the silica is restricted by the presence of the latex.

Initially, film formation is strongly influenced by the volume reduction associated with water evaporation. Knowing the volume fraction of polymer in the latex suspension, the volume of dry polymer produced from a given volume of film can be determined. Equating this with the volume of air accessible to the polymer latex particles in the dry silica powder should yield the critical concentration of silica, where the air between the silica particles and in the pores is exactly replaced by polymer during film formation. At this concentration, the silica packing in the dried lacquer should resemble that in the dry powder.

If the silica in the lacquer packs in a similar way to the dry powder, it should percolate. This forms the primary measure of whether the structure resembles that of the dry powder. However, percolation is necessary but not sufficient in the dry powder; percolation does not imply self-support, but self-support does imply percolation. So the percolation threshold is expected to occur before the critical silica concentration. The percolating structure is shown in Fig. 1(b). At lower silica concentrations, the particles are isolated [Fig. 1(a)] so there is no percolation. Above the critical concentration, silica collapse and densification may occur [Fig. 1(c)], or if a more robust silica structure is formed, air voids may be found, as there is no longer enough polymer to fill the interstices [Fig. 1(d)].

A mathematical description is now presented. The bulk volume V_{bulk}, bulk density ρ_{bulk}, and mass m_{sil} of the dry silica powder are related by

$$V_{bulk}=\frac{m_{sil}}{\rho_{bulk}}. \tag{1}$$

ρ_{bulk} was determined as 62.5 $\mathrm{kg\,m^{-3}}$ by compressing a known mass of silica with a weighted piston (Japanese Industrial Standards association number K6223-1976) [12]. Since the density of silica without included air is 2.18×10^{3} $\mathrm{kg\,m^{-3}}$ [10], there is a large amount of air incorporated into the structure, some as interstices and some as pores ranging in size from a few nanometres to a micron [12].

Here V_{bulk} is the volume of silica and included air, both in pores and between particles. The volume of dry lacquer V_{dry} is given by

$$V_{dry}\approx C_{sol}V_{wet}\frac{\rho_{wet}}{\rho_{dry}}, \tag{2}$$

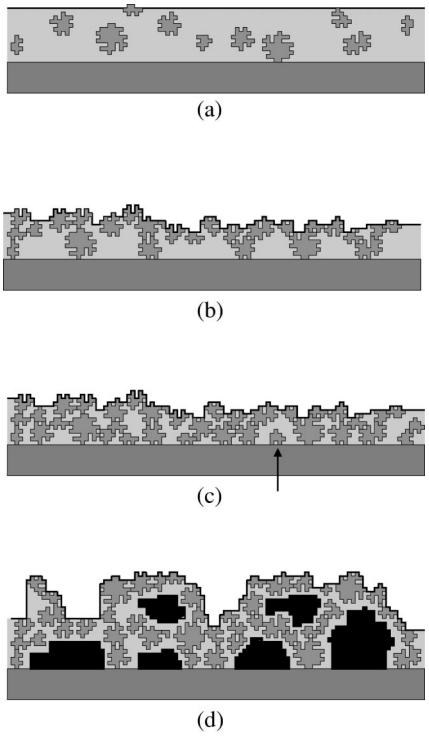

FIG. 1. Schematic of the model of silica structure within dried lacquer. The low concentration regime (a) ($m_{sil}/m_0<1$), critical mass of silica (b) ($m_{sil}/m_0=1$), and two possibilities for $m_{sil}/m_0>1$, with silica densification from collapse (c), or void formation with more robust silica (d). Note that (c) does not exclude the possibility of isolated silica particles: for example, that marked in (c).

with V_{wet} the volume of wet lacquer and $C_{sol}=0.35$ [13] the solids content of this particular system [14]. ρ_{dry} and ρ_{wet} are the densities of the wet and dry lacquers, determined as 1070 and 1023 $\mathrm{kg\,m^{-3}}$, respectively. These values are taken from Table I, for a formulation without silica, as ρ_{dry} should be the density of the polymer binder.

The condition for the critical concentration of silica requires that all air available to the polymer is displaced. The maximum volume available to the latex is the bulk volume occupied by the silica, V_{bulk}, yielding

$$V_{dry}=V_{bulk}, \tag{3}$$

but this neglects the volume that is silica itself, V_{sil} and any pores in the silica particles which are too small for the latex to access, V_{pore}. The volume required to displace the available air is then

$$V_{dry}=V_{bulk}-V_{sil}-V_{pore}. \tag{4}$$

Relating this to the volume of dried lacquer and the bulk and the density of silica without included air gives

$$V_{dry}=m_0\left(\frac{1}{\rho_{bulk}}-\frac{1}{\rho_{sil}}\right)-V_{pore}, \tag{5}$$

where m_0 is the critical mass fraction of silica required to satisfy Eq. (4).

TABLE I. Formulation recipe. The components are added in the order and amounts shown.

Component	Function	Density ($g\,cm^{-3}$)	% by weight in formulation	Supplier
Glascol C47	Latex binder	1.04	71.4	Ref. [13]
Water		1.0	16.8	
Tegofoamex 1488	Defoamer	1.0	0.1	Ref. [15]
Degussa TS100*	Matting agent	2.18	variable	
Dowanol PnB	Coalescing aid	0.9	3.82	Ref. [16]
Dowanol DPnB	Coalescing aid	0.922	1.91	Ref. [17]
Tegofoamex 1488	Defoamer	1.0	0.05	Ref. [15]
Troysol LAC	Anticratering agent	1.04−1.07	0.5	Ref. [18]
Glaswax E1	Surface enhancer	0.995	2.14	Ref. [19]
Henkel DSX 1514	Rheology modifier	1.07	0.8	Ref. [20]

The volume of small pores V_{pore} is a constant for a certain mass of silica, so v^*_{pore}, the volume of pores inaccessible to the latex in 1 kg of silica is introduced. Pores with a diameter less than that of the latex particles (80 nm) are assumed to be inaccessible.

From nitrogen porosimetry, v^*_{pore} was found to be 5.74×10^{-3} $m^4\,kg^{-1}$ [12]. Since $1/\rho_{sil}$ also gives the volume per unit mass, this gives

$$m_0=\frac{V_{wet}C_{sol}\rho_{wet}}{\left(\frac{1}{\rho_{bulk}}-\frac{1}{\rho_{sil}}-v^*_{pore}\right)\rho_{dry}} \tag{6}$$

for the critical mass fraction of silica.

Now, there are air spaces between the silica particles in the dry powder, such that the volume fraction of the silica particles and their pores is equal to the packing fraction p

$$\phi=p. \tag{7}$$

Using Eqs. (1)–(7) gives

$$\phi=p\frac{m_{sil}}{m_0} \tag{8}$$

in the film-formed lacquer where m_{sil}/m_0 is the silica mass fraction.

Equation (8) can be tested by measuring the silica volume fraction ϕ as a function of silica mass added to the lacquer during formulation. It may be valid for $m_{sil}/m_0\leqslant1$ only, if the silica does not collapse at higher concentration, [Fig. 1(d)]. If the silica collapses totally, then ϕ should increase linearly beyond $m_{sil}/m_0=1$ [Fig. 1(c)]. However, $\phi\leqslant1$ by definition, so the linear behavior must be limited.

III. EXPERIMENT

In a confocal laser scanning microscope, light from only one point in the specimen passes through to the detector. All light from other regions in the specimen is rejected by the confocal pinhole. This has the advantage that, provided the sample is reasonably transparent, thick specimens may be imaged without the problem of out-of-focus contributions [5,6].

Since only a single point is observed at any one time, the specimen or light beam must be *scanned* in a similar way to a scanning electron microscope. By scanning vertically as well as horizontally, a 3D image may be produced [6].

The resolution is better than conventional light microscopy, at around 0.1 μm in the horizontal plane, and 0.6 μm in the vertical direction. Selective labeling with a fluorescent dye enormously enhances contrast, by binding it to a region of interest in the specimen. A filter is then used to allow only fluorescent light through to the detector, rejecting reflected light [5]. In order to study matting water-based lacquers, it is therefore necessary to label the silica matting agent with a fluorescent dye. Refractive index matching of the polymer binder with the silica matting agent allows light to penetrate up to 50 μm below the sample surface without significant attenuation. The CLSM used here was a Zeiss LSM 510 fitted with a Zeiss 63× planapochromat objective lens with a 15-mW 488-nm excitation laser.

Sample preparation

The lacquer formulation is shown in Table I. Ingredients are added in the order shown, at 1 min intervals. The silica was dispersed using a Cowles head rotating at 3000 rpm. 15 min of shear followed the addition of the last ingredient.

In order to label the silica for fluorescence mode CLSM work, fluorescein isothiocyanate (FITC) was used. This dye is only sparingly soluble in water, so 1.5 mg were dissolved in 0.1 cm^3 of 0.1-mol sodium hydroxide solution. This alkaline FITC solution was diluted with the water required for the formulation. The silica was then dispersed in this solution prior to mixing. The FITC was assumed to hydrogen bond to the negatively charged silica surface. Since FITC molecules are much smaller than the pore structure of the fumed silica, the dye is assumed to penetrate the pores fully. No loss of brightness is observed between the center and edges of the silica particles (Figs. 5,6), so the dye appears to bind throughout the silica particles.

As the latex binder is alkaline (pH 9), the addition of one drop of 0.1-mol sodium hydroxide to a 50-cm^3 specimen was assumed to have little effect. The FITC concentration was

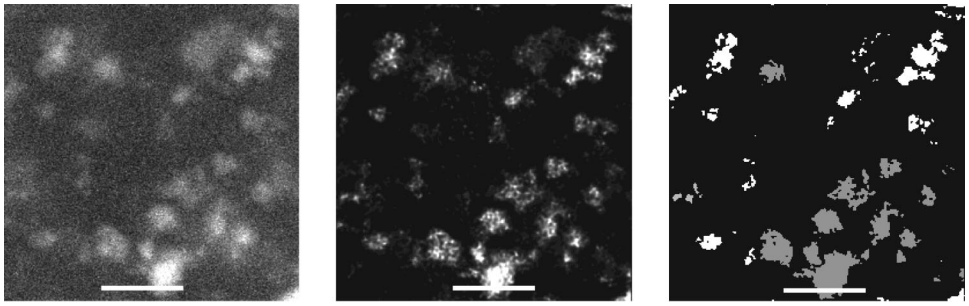

FIG. 2. *xy* images of dried lacquer with silica. (a) Unreconstructed image, (b) EM reconstruction with 100 iterations, (c) segmented image with 3D percolating silica structure shown in white, other silica particles in grey. Bars=4 μm.

held constant throughout, so any changes were associated with the silica. In fact the FITC gives a much stronger signal in the presence of silica, presumably due to adsorption on the silica surface. The silica concentration was varied between $m_{sil}/m_0=0$ and $m_{sil}/m_0=3.0$. The lacquer was laid down on 25-mm square sections of chromated aluminum sheet [21] using a microapplicator [4]. Film thickness was nominally 200 μm, drying to around 60–70 μm after water loss. Film formation was carried out in a dessicator with phosphorous pentoxide dessicant. The specimens were left overnight prior to imaging.

IV. IMAGE ANALYSIS

The image formed in any optical microscope is the convolution of the specimen and a function describing the blurring caused by the microscope [5]. This blurring term is called the point spread function (PSF).

The distribution of FITC (which is taken to be that of the silica) is given by the specimen function. This is obtained by ''deconvolving'' the image with the PSF. A variety of techniques have been developed to tackle this problem [9]. Here the expectation maximization (EM) algorithm of Conchello and co-workers is used [7,8,22]. This iterative method uses a succession of trial specimen functions from which a series of trial images are produced. These trial images are then compared with the measured image, successive iterations are then constrained to approach the specimen function.

In this work the EM algorithm is iterated 100 times. Typical results for dried film containing silica are shown in Figs. 2(a) (original image) and 2(b) (reconstructed specimen function). The improvement in resolution is clear between Figs. 2(a) and 2(b). Conchello *et al.* mention some limitations of the EM method, in particular, the decrease in signal to noise ratio with the number of iterations [8]. However, this is not too apparent in Fig. 2(b) and the images here are all fairly similar, so any limitation of the EM technique should apply to all images equally.

Having obtained the specimen function, silica is separated from the polymer background, as it appears bright in the images. The pixels comprising the images are digitized into integers from 0–255, so by selecting some threshold, the brighter pixels that correspond to silica are found. The fraction of ''bright'' (silica) pixels for images with and without silica is shown in Fig. 3 as a function of threshold. Although the fluorescent signal is much stronger in the presence of silica, there is a residual noise signal in the absence of silica, which requires a brightness threshold to be imposed. As Fig. 3 shows, at a threshold of four, the ''bright pixel fraction'' is between 10^{-4} and 5×10^{-3}. The variation in bright pixel fraction is a result of further noise reduction by constraining the cluster size, as explained below.

To go further, we seek to identify the individual silica particles in an image. At the resolution of the CLSM, it is the aggregate particles that are of interest. At this point, it is important to distinguish silica particles from clusters. A silica particle is a real piece of silica, and a single object. A cluster is a number of neighboring bright pixels in an image, and may correspond to one or more silica particles that lie close together. Since the silica particles are irregular in shape, it is not possible to determine how many particles contribute to each cluster.

Therefore clusters are considered here, and identified with a counting algorithm, which is implemented as follows (Fig. 4). The image is scanned, and if a white pixel (corresponding to a silica particle) is found, a new particle is recorded. Neighboring pixels are tested, and the algorithm moves to the first new white pixel found. Here neighboring pixels are defined as those which share a face, an edge *or* a corner, such that each pixel has 26 neighbors, which corresponds to eight-

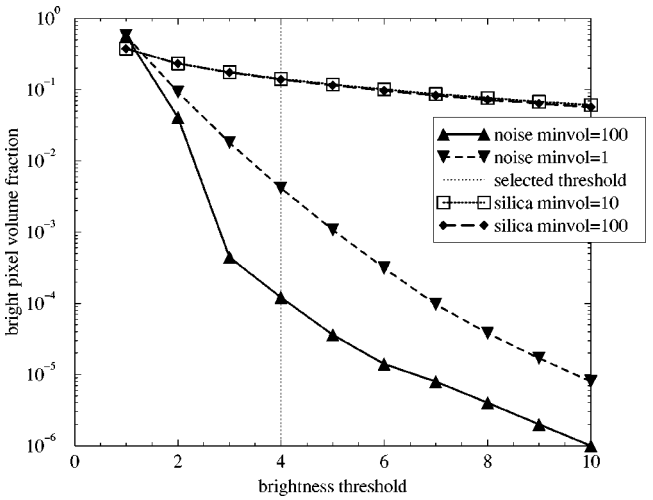

FIG. 3. The selected threshold is the black dotted line, at a brightness of 4. The fraction of bright pixels is shown as a function of threshold. Lines are plotted for images of a silica-containing specimen, and for a specimen without any silica (noise). The minimum cluster volume to be treated as a silica particle is set to 1 and 100 pixels in each case.

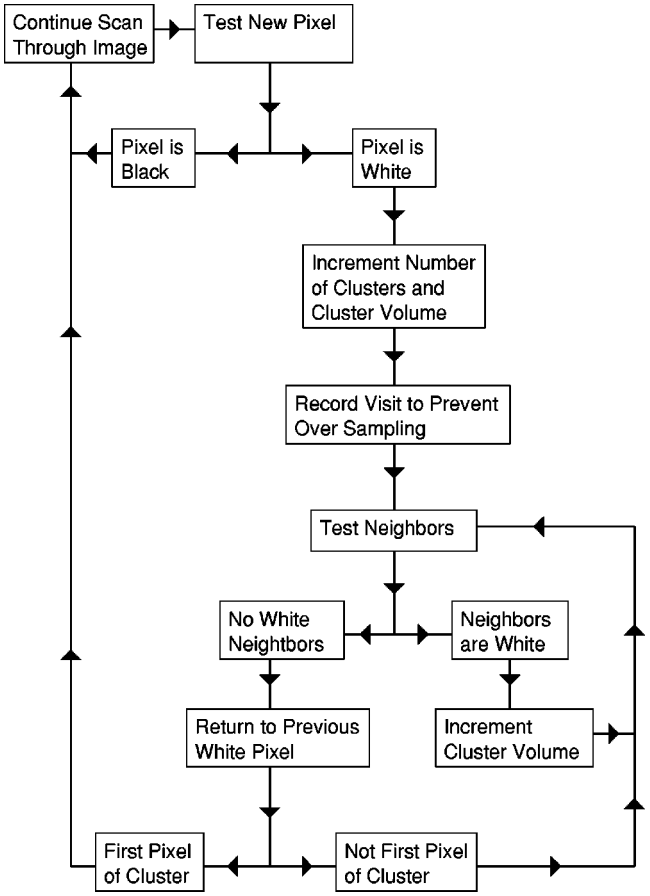

FIG. 4. Algorithm for counting and sizing clusters in a binary image where white corresponds to silica, and black to polymer.

fold connectivity in 2D. The algorithm tests again for neighbors, and moves on if successful. Upon reaching the edge of a cluster of white pixels where no new white neighbors are found, the algorithm returns to the most recent site visited, and moves to the first previously unvisited white neighbor, if possible. Eventually all possibilities are exhausted and the algorithm returns to the first pixel visited and finds no new neighbors. In this way, all the pixels are found, and by incrementing the cluster size for every pixel counted, the volume of each cluster is determined. By labeling each cluster, the number of clusters in a given image may be found.

Knowing the size of each cluster allows further noise reduction, as noise often manifests itself as isolated bright pixels [23], removing these should reduce the noise contribution. By selecting different sizes for this minimum cluster volume (labeled as ''minvol'' in Fig. 3), a cluster volume threshold can be used. Figure 3 shows that imposing a minimum volume of 100 pixels reduces the noise by more than an order of magnitude for a threshold of four. One advantage of this method of noise reduction is that it is non-blurring so does not reduce the resolution of the image at all.

Percolation can be tested directly by comparing cluster labels on opposite sides of the image. If two planes on opposite sides of the image share the same cluster label, then that cluster must span the image. One such cluster is shown in white in Fig. 2(c), although the 3D percolation is not necessarily revealed in 2D, as is the case here.

This cluster labeling enables us to investigate a number of percolation phenomena [24]. The cluster count can be explored as a function of silica concentration. The volume of the largest cluster is also found, which should increase sharply at the percolation threshold.

V. RESULTS AND DISCUSSION

A typical example of the general structure assumed by silica in the bulk of the dry lacquer is shown in Fig. 5 for lateral (a) and vertical (z varying) (b) slices. The data for these images have differing lateral and axial sampling rates of 0.07 μm pixel^{-1} and 0.35 μm pixel^{-1}, respectively. Here the z pixels are expanded by a factor of 5, so that magnification is the same in the x and z directions. Notwithstanding the differing pixel size between the two images, the appearance is very similar, with irregular particles of silica appearing randomly distributed, both laterally and vertically.

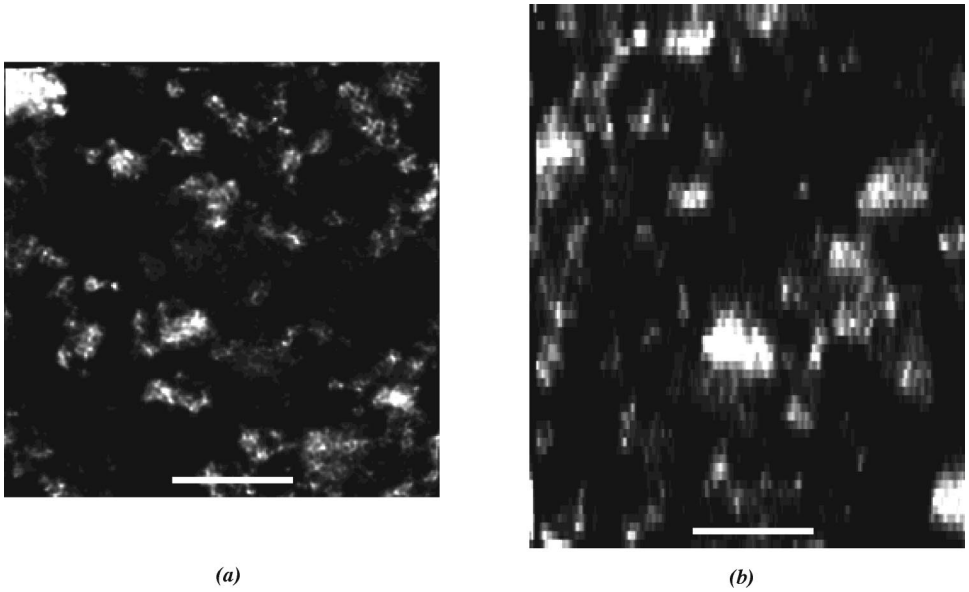

(a) *(b)*

FIG. 5. Confocal microscopy images of lacquer with silica, $m_{sil}/m_0 = 0.94$. Both xy and xz slices are shown in (a) and (b), respectively. The xy slice is taken around 7 μm below the surface. These images have been restored using EM deconvolution. Bar $= 5$ μm. The slice in (a) is 256×256 pixels, whereas (b) is 256×64 pixels with the z pixels expanded such that x and z magnifications are the same. The contrast is enhanced with the color bar shown.

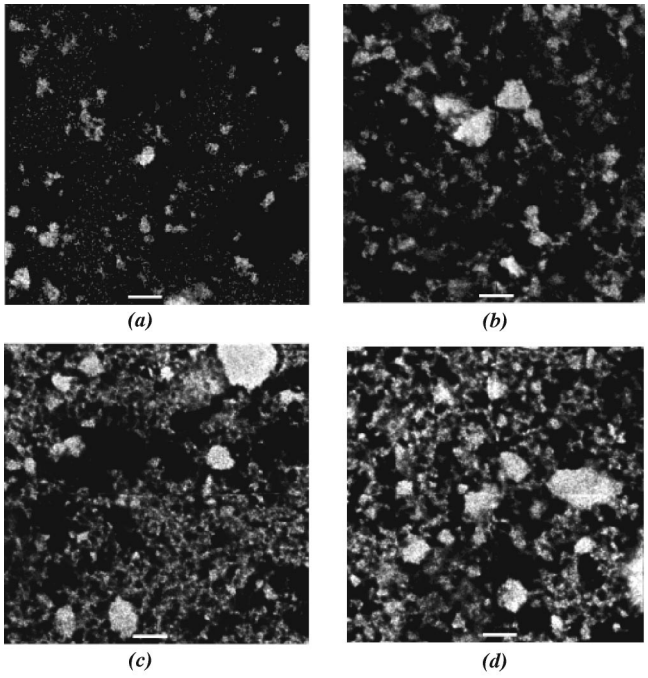

FIG. 6. EM-restored confocal images of film with silica at a range of concentrations. (a) $m_{sil}/m_0=0.47$, (b) $m_{sil}/m_0=0.94$, (c) $m_{sil}/m_0=1.87$, and (d) $m_{sil}/m_0=2.81$. All images are 512×512 pixel xy slices taken at a depth of 7 μm from the surface of the film. Faint horizontal and vertical lines in each image are artifacts of EM restoration of each image in four sections, which are then recombined. Bars=4 μm.

The effect of varying silica concentration is shown in Fig. 6. All of these images are xy planes, taken around 7 μm from the surface. The total film depth is typically 40–50 μm, so these images are well within the bulk. At low concentrations the silica particles are isolated, Fig. 6(a) ($m_{sil}/m_0=0.49$), corresponding to the schematic in Fig. 1(a).

The image shown in Fig. 6(b) has $m_{sil}/m_0=0.98$. Although the silica particles are isolated in two dimensions, using image analysis this structure is found to percolate in 3D. As the silica loading is close to $m_{sil}/m_0=1$, this image corresponds to Fig. 1(b).

Increasing the silica concentration to $m_{sil}/m_0=1.96$ [Fig. 6(c)] reveals percolation in two dimensions. There is rather more silica present than in the previous image, which is indicative of silica densification associated with structural collapse, corresponding to Fig. 1(c). At higher loading still [$m_{sil}/m_0=2.93$, Fig. 6(d)], there is more densification, with silica present throughout the image.

Quantitative results

We now consider quantitative analysis of these images, first looking at the effect of silica volume fraction before moving on to percolation phenomena. The total proportion of pixels brighter than the threshold is the silica volume fraction, ϕ. ϕ is plotted as a function of m_{sil}/m_0 in Fig. 7. Each point in the plot is the mean of 1–6 images (typically 4). Error bars are the standard error. From the plot ϕ is revealed to be a reasonably linear function of m_{sil}/m_0. The slope of the plot is equal to the packing fraction p from Eq. (8). Of course, this straight line behavior is limited in extent, because $\phi\leqslant1$. The values obtained from a regression fit of the data in Fig. 7 give $p=0.145\pm0.013$ and an intercept of 0.012 ± 0.019. The intercept is equal to zero within error bounds, as expected from Eq. (8).

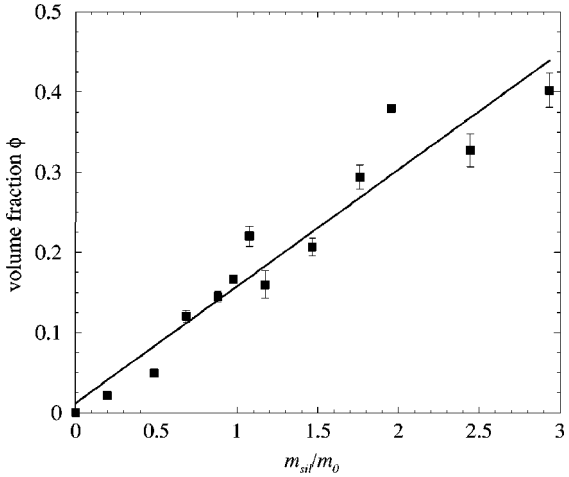

FIG. 7. Silica volume fraction as a function of m_{sil}/m_0, determined from confocal images. This plot is a direct realization of Eq. (3.10). The value of the packing fraction p is found with a regression fit.

The fact that $\phi(m_{sil}/m_0)$ is linear well beyond $m_{sil}/m_0=1$ means that the silica structure must collapse [Fig. 1(c)]. Any noncollapsing structure should plateau as a function of m_{sil}/m_0, which is not seen. Adding more silica simply results in a denser structure.

The silica volume fraction can also be plotted as a function of depth. In particular, this should reveal whether or not there is more silica present towards the surface than in the bulk of the film. Some of the data is plotted in Fig. 8, and there is generally little consistent variation with depth, although there are some local fluctuations, which is in agreement with the assumption that the silica is uniformly distributed throughout the lacquer.

The percolation threshold of the silica structure is found directly from image analysis. Percolation is central to the expected silica behavior. Recall that the silica should percolate for $m_{sil}/m_0\lesssim1$, to support the concept of a silica structure essentially unaltered by the addition of lacquer at the critical silica concentration. These data, however, come with a health warning: the system is very small for observing percolation, relative to the size of the silica particles. It is treated as a semi-infinite system, when in fact the image size is $512\times512\times64$ pixels (35 μm$\times$35 μm$\times$24 μm). Nonetheless, percolation is directly tested in three dimensions with the algorithm described above. The threshold is taken from the lowest concentration of silica that consistently exhibited percolation. The next-lowest concentration, $m_{sil}/m_0=0.88$, occasionally percolated, but $m_{sil}/m_0=0.98$ almost always did. In effect this gave a range, that the percolation threshold fell between $m_{sil}/m_0=0.88$ and $m_{sil}/m_0=0.98$, which is close to the value of unity where the silica structure should resemble that of the dry powder, and percolate.

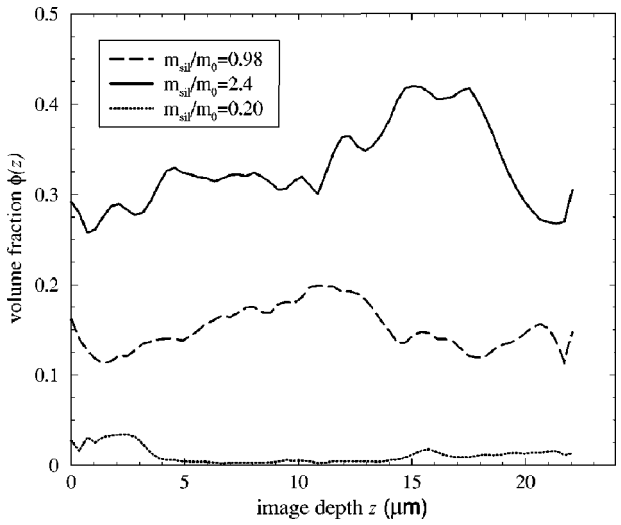

FIG. 8. Silica volume fraction as a function of depth. Various silica concentrations are shown. Apart from local fluctuations, the lines are fairly uniform, with no tendency for surface segregation. Results for three typical images are shown.

Percolation can also be considered through the variation in the number of clusters as a function of m_{sil}/m_0. At low silica concentration the cluster count increases with m_{sil}/m_0, until enough silica particles touch that it rises more slowly as a function of m_{sil}/m_0. Eventually, the count is expected to peak, a little before percolation [24]. Ultimately at high silica volume fraction, the cluster count will decline to a low value as eventually all the silica in the image is part of the same large cluster.

Such behavior with a clear peak is shown in Fig. 9. Again, each point is the mean of typically four images, with error bars the standard error. The large error is taken to be due to the small system size.

The equivalent count on a randomly populated $256\times256\times64$ cubic lattice was also found. The lattices produced were treated by the same image analysis technique as

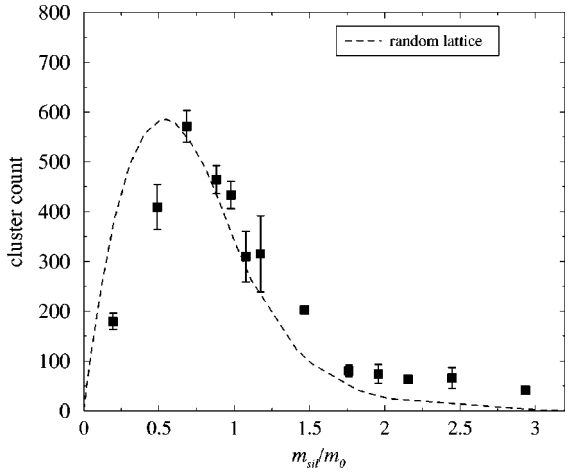

FIG. 9. Cluster count as a function of m_{sil}/m_0. Dotted line is the count on a randomly populated $256\times256\times64$ cubic lattice, normalized to the experimental peak and scaled to m_{sil}/m_0.

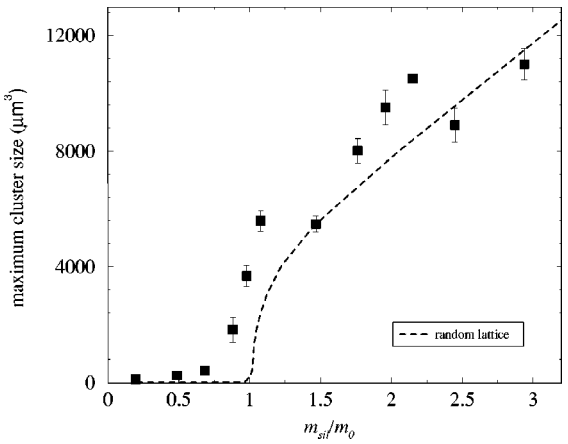

FIG. 10. Maximum cluster size as a function of m_{sil}/m_0. At the percolation threshold, the maximum cluster size increases discontinuously. Further increase in cluster size is the result of densification. Dotted line is the maximum cluster size on a $256\times256\times64$ lattice.

the experimental work to produce cluster counts and look for the percolation threshold. The random lattice has a percolation threshold at a volume fraction of around 0.091. The volume fraction values are therefore scaled by a factor of 0.135/0.091 since 0.135 $(=p\times0.93)$ is the silica volume fraction in the middle of the range obtained for the percolation threshold. This scaling is justified because the cluster count is a function of percolation rather than absolute volume fraction. Different percolation thresholds are not surprising between the regular cubic lattice and irregularly shaped silica particles [24].

The scaled volume fraction values are divided by the packing fraction p to obtain the count as a function of m_{sil}/m_0 from Eq. (8). The random lattice data is then plotted as a function of m_{sil}/m_0 with the count values normalized to the experimental work, in Fig. 9. Considering the simplicity of the randomly populated cubic lattice, the agreement with experimental data is good.

A third test of percolation uses the measure of the largest cluster (Fig. 10). Here size is measured as the number of pixels comprising the largest cluster, which is explicitly evaluated in μm^3. This size is clearly limited to the volume of specimen sampled to form the image, 28 800 μm^3. Below the percolation threshold, the clusters are small, corresponding to isolated silica particles. The volume then increases sharply around the percolation threshold as the largest cluster now corresponds to many silica particles. This increase would be discontinuous in a large system [24]. Further increase with densification is seen at high m_{sil}/m_0 values, as the volume of the largest cluster increases with rising silica volume fraction.

Again the experimental data show the same trend as the random lattice simulation. The x values were scaled as above, and the y values were normalized in accordance with experiment. Although there is the same general behavior as the experimental data, the larger size of the silica particles compared to the single pixels of the random lattice is particularly apparent at low m_{sil}/m_0.

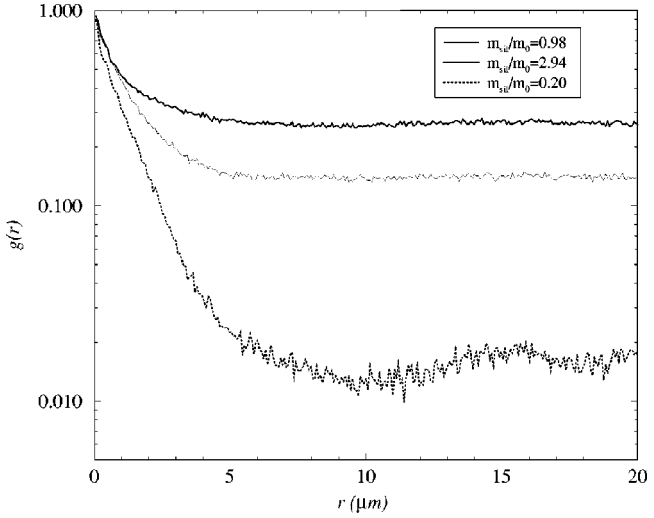

FIG. 11. Pair correlation function. $g(r)$ is found by randomly sampling pixels from pixel identified as silica. Results for three typical images are shown.

The typical size of the aggregated silica particles can be found using the pair correlation function $[g(r)]$, Fig. 11. It is not possible to define the centers of the aggregate particles, due to their irregular shape. Therefore the $g(r)$ is calculated as the probability that a pixel a distance r from a pixel known to be ''silica'' is also ''silica.'' To save computer time, the pair correlation function is determined by randomly sampling 10^4 pixels per one pixel interval, rather than measuring the seperation of every pair of pixels.

The absence of a peak in Fig. 11 suggests a disordered structure, as would be expected from the images in Fig. 6. The correlation decays to the background level (the silica volume fraction) over a length scale of 5 μm, which may be taken as an upper bound for the silica particle size. The pair correlation function supports the notion that the structure is homogenous on length scales greater than the aggregate silica particles.

We do not believe that Fig. 11 shows any change in length scale with volume fraction. Although the $m_{sil}/m_0=0.20$ line appears to have a slightly longer tail-off, this is taken to be due to faster truncation at higher silica volume fraction.

VI. CONCLUSIONS

The structure of silica in the bulk of matt water-based lacquers has been investigated with confocal microscopy. Using image analysis, three structures are identified, at different silica concentrations: separated silica particles $(m_{sil}/m_0<1)$, percolation, $(m_{sil}/m_0\approx1)$, and collapsed $(m_{sil}/m_0>1)$.

At low concentrations $(m_{sil}/m_0<1)$, the aggregate silica particles are dispersed throughout the lacquer, with no tendency for surface segregation. We have assumed a critical silica concentration, where the silica structure should be similar to that found in the dry powder. At this point $(m_{sil}/m_0=1)$, the silica particles should no longer be isolated, but should form a percolating structure. The percolation threshold was found at a silica concentration in agreement with the model.

At higher silica concentrations, the structure is rather denser, with higher silica volume fraction. Since the bulk volume of silica for $m_{sil}/m_0>1$ exceeds that of the dried film, the densification is taken to be collapse of the silica structure due the volume reduction in film formation. This collapsing structure is entirely consistent with weakly bound fumed silica.

[1] J.L. Keddie, Mater. Sci. Eng., R. **21**, 101 (1997).
[2] H. Schneider, Surf. Coat. Int. **77**, 376 (1994).
[3] L. Gate, W. Windle, and M. Hine, Tappi. J., **56**, 61 (1973).
[4] C.P. Royall and A.M. Donald, *Film Formation in Coatings: Mechanisms, Properties, and Morphology*, edited by T. Provder and M. Urban, ACS Symposium Series Vol. 790 (ACS, Washington, DC, 2001).
[5] J.B. Pawley, *Handbook of Biological Confocal Microscopy*, 2nd ed. (Plenum, New York, 1995).
[6] C.J.R. Sheppard and D.M. Shotton, *Confocal Laser Scanning Microscopy*, Microscopy Handbooks Vol. 38 (BIOS Scientific, Oxford, UK, 1997).
[7] J-A. Conchello and J.G. McNally, Proc. SPIE **2655**, 198 (1996).
[8] J. Markham and J.-A. Conchello, Proc. SPIE **2655**, 18 (1997).
[9] J.G. McNally, C. Preza, J-A. Conchello, and L.J. Thomas, Jr., J. Opt. Soc. Am. A **11**, 1056 (1994).
[10] R.K. Iler, *The Chemistry of Silica* (Wiley, New York, 1979).
[11] P. Kleinschmidt, R. Soc. Chem. **40**, 196 (1981), special publication.
[12] G. Morea-Swift (private communication).
[13] Glascol C47, Technical and Processing Data, Allied Colloids, Coatings and Specialities Division, Bradford, UK.
[14] G.P.A. Turner, *Introduction to Paint Chemistry*, 3rd ed. (Chapman and Hall, London, 1991).
[15] TEGO Foamex 1488 safety data sheet, Tego Chemie Service, Th. Goldschmidt Ltd., Chippenham, Kinston, Milton Keynes, Bucks, MK10 0AE, U.K.
[16] Dowanol PNB glycol ether safety data sheet, Univar PLC, Suffolk House, George St., Croydon, CR9 3QL, U.K.
[17] Dowanol DPNB glycol ether safety data sheet, Univar PLC, Suffolk House, George St., Croydon, CR9 3QL, U.K.
[18] Technical Data, Troysol LAC, Troy Chemical Co., Adelphi mill, Grimshaw ln, Bollington, Macclesfield, U.K.
[19] Glaswax E1, Technical and Processing Data, Allied Colloids, Coatings and Specialities Division, Bradford, U.K.
[20] Henkel Performance Chemicals, DSX 1524, 147 Kirkstall Rd., Leeds, LS2 1JN, U.K.
[21] S. Wernick and R. Pinner, *Surface Treatment of Aluminium*, 4th ed. (Clare o' Moseley Ltd., Moseley, Surrey, U.K, 1972).
[22] S.F. Gibson and F. Lanni, J. Opt. Soc. Am. A **8**, 1601 (1991).
[23] J.C. Russ, *The Image Processing Handbook*, 2nd ed. (CRC, Boca Raton, 1995).
[24] D. Stauffer and A. Aharaony, *Introduction to Percolation Theory*, 2nd ed. (Taylor & Francis, London, 1992).